EES Solar

Accepted Manuscript

This article can be cited before page numbers have been issued, to do this please use: W. Zia, M. M. Byranvand, V. Yeddu, Y. Haruta, D. Zhang, M. Saidaminov and M. Saliba, *EES Sol.*, 2025, DOI: 10.1039/D5EL00087D.

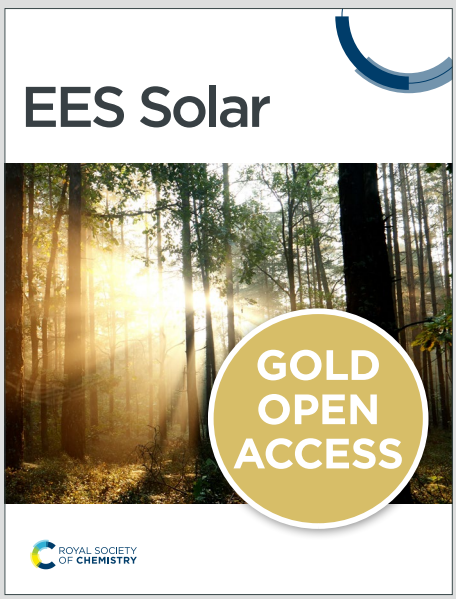

View Article Online
DOI: 10.1039/D5EL00087D

Broader Context

While narrow-bandgap perovskites have been central to the development of high-efficiency solar cells, wide-bandgap counterparts, like $MAPbCl_3$, are gaining interest. Its inherent transparency and the ability to yield high open-circuit voltages make it well-suited for applications like smart windows and advanced sensor systems, which can operate at very low current inputs. However, achieving a uniform polycrystalline $MAPbCl_3$ defect-free thin film remains a significant challenge. We have demonstrated that growing single-crystalline thin films of $MAPbCl_3$ via inverse temperature crystallization results in highly crystalline thin films with minimal deep trap states, without requiring post-treatment. Apart from employing these single-crystalline $MAPbCl_3$ thin films for the first time as solar cells, we also extend their use to X-ray voltaic devices. Notably, under X-ray exposure, wide-bandgap perovskites outperform their narrow-bandgap perovskites, an inverse trend compared to performance under solar illumination. This broadens the scope of $MAPbCl_3$ beyond traditional photovoltaics, like industrial inspection, space radiation monitoring, and medical diagnostics. These diverse functionalities play a vital role in the commercialization of perovskites.

View Article Online
DOI: 10.1039/D5EL00087D

Single-Crystalline $MAPbCl_3$ Thin-Films for Photo- and X-ray Voltaics

Waqas Zia[1,2], Mahdi Malekshahi Byranvand[1*], Vishal Yeddu[3], Yuki Haruta[3], Dongyang Zhang[3], Makhsud I. Saidaminov[3,4*], Michael Saliba[1,2*]

[1]*Institute for Photovoltaics (ipv), University of Stuttgart, 70569 Stuttgart, Germany*

[2] *Helmholtz Young Investigator Group FRONTRUNNER, IMD-3 Photovoltaics, Forschungszentrum Jülich, 52425 Jülich, Germany*

[3]*Department of Chemistry, University of Victoria, 3800 Finnerty Road, Victoria, British Columbia V8P 5C2, Canada*

[4]*Department of Electrical & Computer Engineering, University of Victoria, 3800 Finnerty Road, Victoria, British Columbia V8P 5C2, Canada*

Abstract:

3 eV wide bandgap methylammonium lead trichloride ($MAPbCl_3$) perovskites are promising for transparent solar cells, smart windows, and Internet of Things (IoTs). However, it is challenging to crystallize uniform polycrystalline $MAPbCl_3$ thin films from solution. On the other hand, single-crystalline $MAPbCl_3$ can be deposited as relatively uniform thin films. In this work, we demonstrate the fabrication of single-crystalline $MAPbCl_3$ thin films on conductive glass substrates via a space-confined inverse temperature crystallization (ITC). The perovskite films exhibit no emission peaks from states located deep within the bandgap, confirming a less defective perovskite bulk than its polycrystalline counterpart. The resulting perovskite solar cells (PSCs) yield open-circuit voltage (V_{OC}) of up to 1.64 V and a record power conversion efficiency (PCE) of 1.1 % under one sun irradiation. Additionally, the $MAPbCl_3$ is studied for its conversion of X-rays into electrical energy, i.e., "X-ray-voltaics", demonstrating a V_{OC} of 0.89 V together with an output power of 3.57 μW cm^{-2} at an X-ray tube voltage of 60 kV (4900 μW cm^{-2}).

View Article Online
DOI: 10.1039/D5EL00087D

Introduction

Metal-halide perovskite solar cells (PSCs) have attracted much attention in recent years due to their excellent optoelectronic properties[1–4] based primarily on polycrystalline perovskite thin films. Despite their excellent progress in power conversion efficiencies (PCEs), the open-circuit voltage (V_{OC}) deficit for wide bandgap perovskites still needs to be minimized.[5–7]

Recently, we have reported among the highest V_{OC} of 1.78 V for single-junction PSCs based on methylammonium lead chloride ($MAPbCl_3$).[8] However, considering the wide bandgap (E_g) of 3.03 eV for $MAPbCl_3$, there is still a significant loss-in-potential (i.e., $E_g/q - V_{OC}$) since the potential V_{OC} for $MAPbCl_3$ is 2.69 V (corresponding to a loss-in-potential of 0.34 V).[9] Our work has shown that the crystallization of $MAPbCl_3$ thin films with a homogenous morphology and a uniform interface is quite challenging because of the lower solubility of chloride salts in organic solvents and fast crystallization kinetics. This results in excessive non-radiative recombination, leading to a significant loss-in-potential.[8]

However, the solution-grown cubic and transparent bulk $MAPbCl_3$ single crystals have been used for photodetector applications.[10,11] On a similar basis, various PSCs based on single-crystalline films have been demonstrated using various perovskites, e.g., $MAPbI_3$ (1.55 eV), $MAPbBr_3$ (2.3 eV), $FA_{0.6}MA_{0.4}PbI_3$ (1.48 eV), and $FAPbI_3$ (1.5 eV).[12–15] However, in contrast to bulk perovskite single crystals, which are many cm's in size, growing single-crystalline films on the substrate is challenging because of unwanted nucleation sites, control of thickness, and growth dynamics. One method for answering these challenges is the space-confined inverse temperature crystallization (ITC) method that has been used for single-crystalline thin films.[16,17]

These single-crystalline thin films, due to their relatively high thicknesses, can effectively absorb high-energy neutrons, alpha (α) particles, beta (β) particles, and X-rays.[18,19] Thus, they might find applications to convert the radiant energy of these high-energy particles and radiation into electrical energy. Zhao and co-workers have demonstrated β-voltaics based on polycrystalline $MAPbBr_3$ and mixed-cation PSCs. These β-voltaic cells find their applications in space electronics and implantable medical devices due to their long lifespan, high energy density, and durability.[20,21] In contrast, X-rays offer better energy conversion owing to their higher penetration depth than β-particles. Recently, $MAPbI_3$ single-crystalline solar cells have been tested as X-ray voltaic devices.[22]

View Article Online
DOI: 10.1039/D5EL00087D

A sufficiently thick perovskite film with a wide bandgap is needed to absorb high-energy particles, enhance their energy deposition, and minimize thermal losses. Polycrystalline perovskite thin films are typically limited to ~1 μm, which may hinder their applicability. On the other hand, single-crystalline perovskite films address these challenges as they are free of grain boundaries, have high charge mobilities, and are relatively thick.[23–26] Here, single-crystalline $MAPbCl_3$ thin film is of particular interest because its wide bandgap reduces the thermal losses from high-energy particles. In addition, single-crystalline $MAPbCl_3$ films can be crystallized without annealing or post-treatment steps to improve the film morphology. These single-crystalline $MAPbCl_3$ thin films can be integrated into X-ray voltaic cells to absorb high-energy X-rays, suitable for applications like security screening, flaw detection, and environmental monitoring.[27]

Here, among the first time, we fabricate single-crystalline $MAPbCl_3$ thin films via the space-confined ITC method for both photovoltaic and X-ray voltaic applications. The fabricated device, without any passivation or post-treatment steps, shows a V_{OC} of 1.64 V with a record PCE of 1.1%, under one sun illumination. Despite high crystalline quality and absence of grain boundaries, a higher V_{OC} compared to passivated polycrystalline thin films (a few hundred nm's thick) has not been achieved. This can be related to the higher thickness of single-crystalline films (a few μm's thick), which may result in higher saturation current density due to excessive non-radiative recombination processes. Accordingly, these solar cells are further employed as X-ray voltaic cells: at an X-ray tube voltage of 60 kV (equal to an input power density of 4900 μW cm^{-2}), a V_{OC} of 0.89 V is obtained along with an output power density of 3.57 μW cm^{-2}. According to the best of our knowledge, this is the highest power conversion achieved by X-rays for perovskite solar cells. These initial results show that by carefully optimizing the crystallization process and thickness of $MAPbCl_3$, an alternative use case can be established for such widest bandgap materials.

Results and Discussion

Single-crystalline $MAPbCl_3$ thin films are grown by the space-confined ITC method.[16,17] The experimental details can be found in the supplementary information (SI). Briefly, the perovskite precursor solution is sandwiched between two substrates, and the temperature is increased slowly to 100 °C (Figure 1a). When the solution reaches the supersaturation limit, a single-crystalline thin film grows within the confined space.

View Article Online
DOI: 10.1039/D5EL00087D

We note that single-crystalline $MAPbCl_3$ films form without any additional annealing or passivation step at ambient conditions in air. This is confirmed by the crystallographic properties of the obtained $MAPbCl_3$ films via X-ray diffraction (XRD), showing intense reflections at (100), (200), and (300) planes at diffraction angles of 15.59°, 31.50°, and 47.98°, respectively. There is no additional diffraction response from other planes (Figure 1b). When compared to our previously reported polycrystalline $MAPbCl_3$ thin films,[15] additional multiple reflections from different planes can be observed at 22.12°, 35.32°, and 38.78°.

For the optical properties, photoluminescence (PL) measurements for both single and polycrystalline thin films are performed. Figure 1c shows the band-to-band radiative recombination peaks at 406 nm in both cases. For the polycrystalline thin film, an additional peak can be observed at 750 nm, indicating a band-to-defect recombination peak. Consistent with our previous findings, this peak confirms the existence of deep defect states in the polycrystalline $MAPbCl_3$ perovskite.[8]

On the other hand, this additional peak has not been observed for the single-crystalline sample, which is consistent with the absence of deep traps due to fewer defects in the bulk. However, the asymmetry of the PL spectrum for single-crystalline $MAPbCl_3$ has already been reported in the literature and is attributed to the presence of Cl^- vacancies at the crystal surface.[11] This highlights the fact that, due to its lower formation energy (-0.7 eV) compared to iodine (-0.1 eV) and bromine (0.25 eV) -based counterparts, $MAPbCl_3$ is intrinsically prone to surface defects.[28]

The UV-Vis absorption spectra of single- and polycrystalline thin films are illustrated in Figure 1c (inset). The extracted Tauc plot of single-crystalline thin film shows a slightly lower bandgap of 2.98 eV compared to polycrystalline thin film (3.06 eV) (see Figure S1 in the SI), which follows the reported bandgap values for single-[29] and polycrystalline[30] $MAPbCl_3$ thin films. The narrowing of the bandgap for perovskite single crystals due to their thickness-dependent below-bandgap absorption is well reported in the literature and attributed to the slight transition of direct bandgap to indirect bandgap.[31–33] It has been argued that, for thicker perovskite films, this transition happens due to the distortion of the lead iodide framework. This results in an electric field across the Pb atom and, hence, splits the conduction band via Rashba splitting.[34]

View Article Online
DOI: 10.1039/D5EL00087D

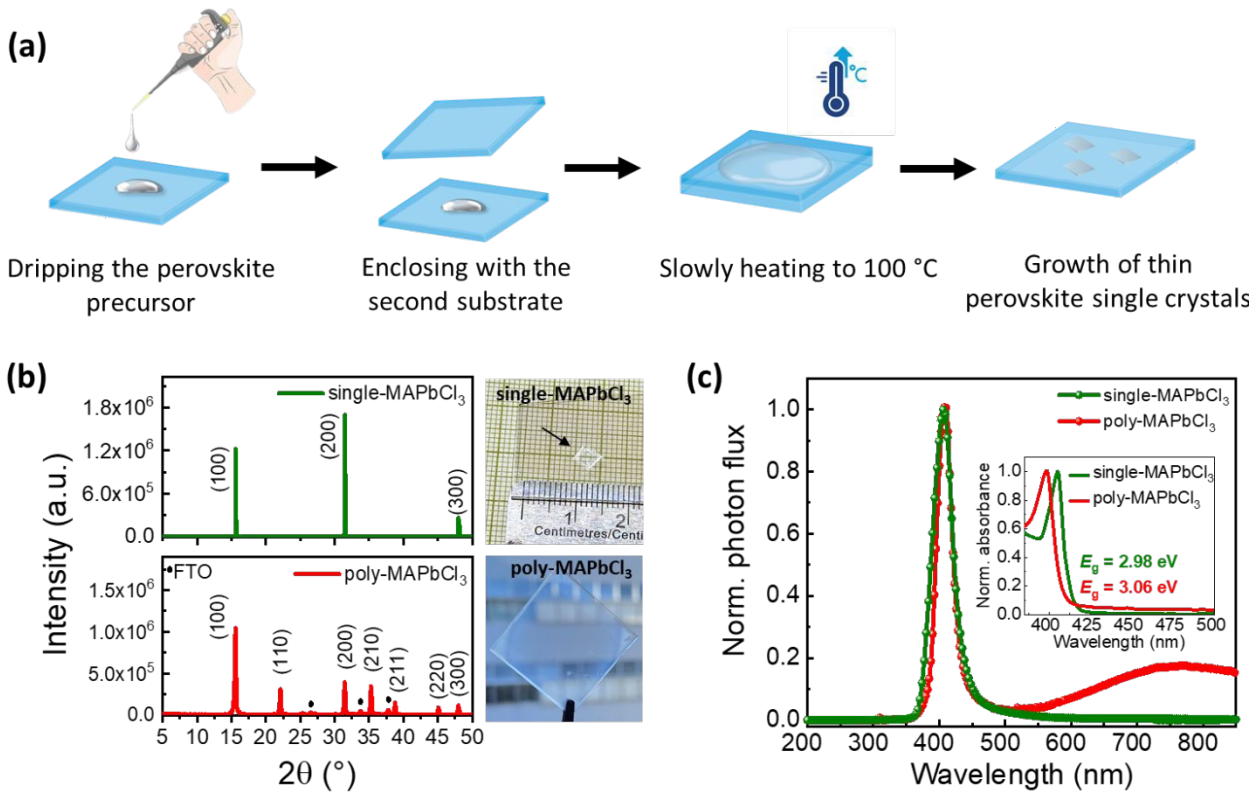

Figure 1. (a) Schematics show the steps in fabricating single-crystalline $MAPbCl_3$ solar cells via space-confined ITC. (b) XRD spectra of the single-crystalline and polycrystalline $MAPbCl_3$ thin films. (c) Normalized PL spectrum of the single-crystalline and polycrystalline thin film measured at an excitation wavelength of 343 nm (inset: normalized absorbance spectra showing a bandgap of 2.98 eV).

In the next step, we incorporate the single-crystalline films into solar cell stacks of glass/ITO/SnO_2/$MAPbCl_3$/Spiro-OMeTAD/Au. Figure 2a shows a photograph of a single-crystalline $MAPbCl_3$ solar cell (see the Experimental Section in SI). On the other hand, polycrystalline $MAPbCl_3$ solar cells are fabricated using a layer stack glass/FTO/c-TiO_2/mp-TiO_2/$MAPbCl_3$/Spiro-OMeTAD/Au as described in our previous work.[8] We note that due to the poor film coverage of polycrystalline $MAPbCl_3$ films, planar SnO_2 electron transport layer (ETL) always leads to shunting paths, resulting in non-functional devices, as shown in Figure S2. Owing to this, a mesoporous TiO_2-based ETL is required to avoid shunting, as its mesoporous structure embeds the perovskite efficiently. However, the same mesoporous TiO_2 layer might not provide a smooth surface for the growth of single-crystalline thin films, as the underlying mesoporous film would induce unwanted heterogeneous nucleation sites, hampering the formation of single

View Article Online
DOI: 10.1039/D5EL00087D

crystals.[35] Hence, a facile, planar SnO_2 ETL on an ITO substrate is needed to achieve high-quality single-crystalline $MAPbCl_3$ films.

Figure 2b shows the statistical data of the photovoltaic parameters for both single- and polycrystalline solar cells with 8 devices in each case under one sun. The single-crystalline devices show remarkable reproducibility with average V_{OC} = 1.59 ± 0.03 V, short-circuit current density (J_{SC}) = 1.09 ± 0.11 mA cm^{-2}, a fill factor (FF) = 67.6 ± 3.66 % and a PCE = 1.11 ± 0.08 %. On the other hand, polycrystalline devices show an average V_{OC} of 1.52 ± 0.05 V, J_{SC} = 0.46 ± 0.08 mA cm^{-2}, FF = 51.5 ± 5.73 %, and PCE = 0.36 ± 0.10 %.

The champion single-crystalline $MAbCl_3$ solar cell results in a V_{OC} of 1.64 V, J_{SC} of 0.9 mA cm^{-2} and FF of 74.5% with a PCE of 1.10%. To the best of our knowledge, this represents the highest reported PCE for $MAPbCl_3$ solar cells. On the other hand, the champion polycrystalline $MAPbCl_3$ solar cell has yielded a lower V_{OC} of 1.58 V, J_{SC} of 0.59 mA $cm^{-2,}$ and FF of 60.2%, leading to a significantly lower PCE of 0.56% (See Figure 2c, Table 1). Since V_{OC} is the main performance criteria for these wide bandgap perovskites with significantly lower currents, we perform long-term V_{OC} tracking on these devices. Figure 2d shows stabilized V_{OC} for 500 s under constant illumination for both single- and polycrystalline $MAPbCl_3$ thin films, highlighting their significant long-term stability.

View Article Online
DOI: 10.1039/D5EL00087D

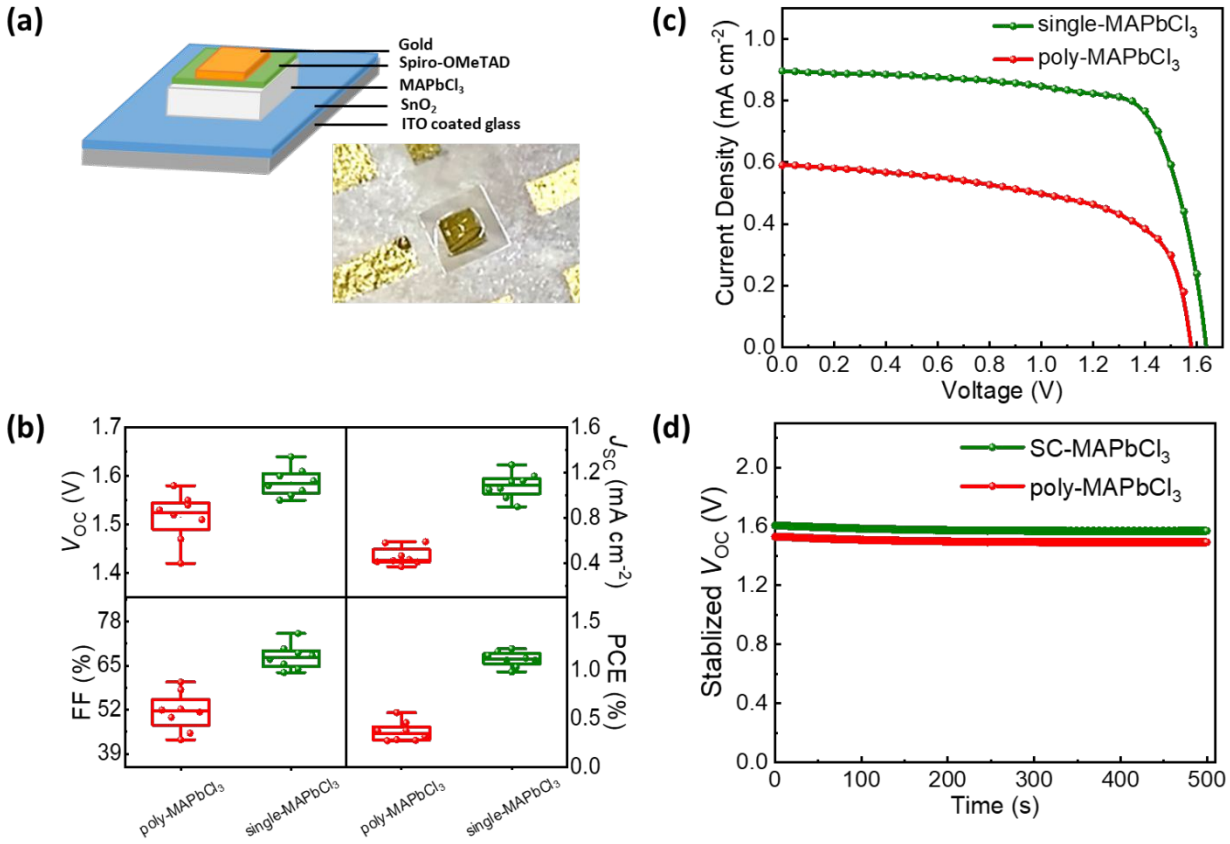

Figure 2 (a) Layer stack of a single-crystalline $MAPbCl_3$ solar cell with a n-i-p configuration, together with a photograph of a single-crystalline $MAPbCl_3$ solar cell (b) Device statistics for V_{OC}, J_{SC}, FF, and PCE of single-crystalline and polycrystalline $MAPbCl_3$ solar cells (n = 8 devices). (c) *JV*-curve of the champion solar cells. (d) Stabilized V_{OC} for 500 s for both single- and polycrystalline $MAPbCl_3$ solar cells.

Table 1 Photovoltaic parameters of single- and polycrystalline $MAPbCl_3$ solar cells

	V_{OC} (V)	J_{SC} (mA cm^{-2})	FF (%)	PCE (%)
poly-$MAPbCl_3$	1.58	0.59	60.2	0.56
single-$MAPbCl_3$	1.64	0.90	74.5	1.10

Although the single-crystalline $MAPbCl_3$ thin films grown by the space-confined ITC method are of high quality in terms of their crystallinity and optical properties, still, a V_{OC} of 1.64 V is lower than the theoretical limit of 2.69 V for a E_g of ~ 3.1 eV, as reported by Lunt et al.[9]

In our previous work on polycrystalline $MAPbCl_3$ thin films, annealing of the films in MACl vapor atmosphere has resulted into an improved film morphology, leading to a V_{OC} of 1.78 V.[8] Such post

View Article Online
DOI: 10.1039/D5EL00087D

-treatments in various annealing atmospheres for a prolonged annealing at high temperatures result in the detachment of the single crystals, leading to no electrical contact between $MAPbCl_3$ and the SnO_2 ETL. However, one of the main reasons for the lower V_{OC} is the higher thickness of single-crystalline thin films, as polycrystalline perovskite thin films grown by spin-coating are typically a few hundred nanometers thick, whereas single-crystalline thin films are usually a few µm's thick. Figures 3 (a) and (b) show the cross-section scanning electron microscope (SEM) images of two different single-crystalline $MAPbCl_3$ thin film solar cells consisting of ITO/SnO_2/$MAPbCl_3$/spiro-OMeTAD/Au layer stack. These images show that the thickness of single-crystalline $MAPbCl_3$ thin films ranges from 4 µm to 18 µm. The diffusion of charge carriers toward the surface of a semiconductor becomes less efficient if the surface lies further away.[36]

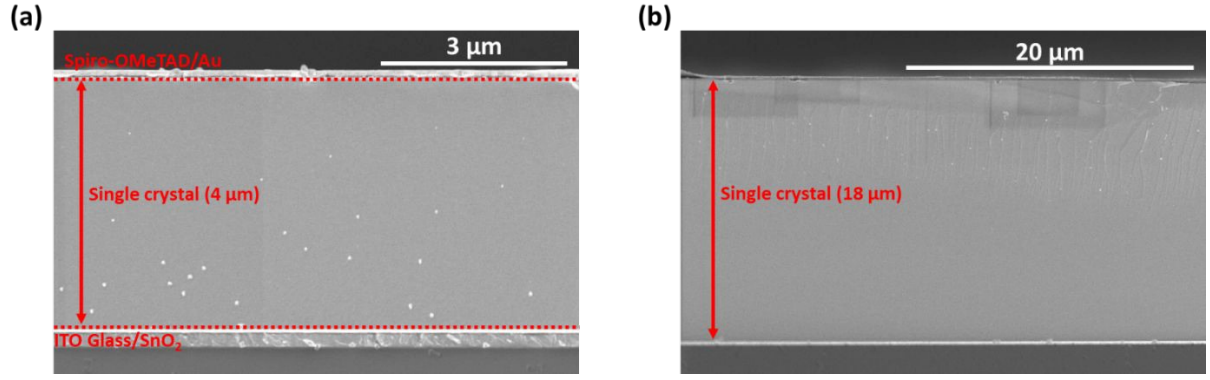

Figure 3 SEM cross-section of a single-crystalline $MAPbCl_3$ thin film solar cell (a) single-crystalline thin film with a thickness of~4 µm (b) single-crystalline thin film with a thickness of~18 µm.

This can be further explained with the help of the diode equation for a single junction solar cell ($V_{OC} = \frac{nkT}{q}\ln\left(\frac{J_{SC}}{J_0}+1\right)$), where n is the ideality factor, k is Boltzmann constant, T is the temperature, and J_{SC} and J_0 are the photogenerated and saturation current densities, respectively. The increase in the saturation current density J_0 is generally correlated with the increase in non-radiative recombination in a solar cell and, hence, a decrease in the V_{OC}.[37,38] Kirchartz and co-workers have reported that J_0 within the bulk increases linearly with the increase in the absorber layer thickness. With a thicker perovskite layer, more photons can be absorbed, and hence, more photogenerated charge carriers are produced. However, at the same time, it triggers more non-radiative recombination mechanisms within the perovskite bulk, which leads to significant V_{OC}

View Article Online
DOI: 10.1039/D5EL00087D

losses.[39,40] Huang and his team have shown a decrease in the V_{OC} of single-crystalline $MAPbI_3$ solar cells with an increase in the thickness of single-crystalline thin films up to 40 µm. Similarly, Turedi et al. demonstrated that increasing the thickness of the perovskite layer in single-crystalline solar cells led to a decline in device performance, attributed to inefficient charge carrier collection.[31,41]

One aspect of this lower V_{OC} is the narrowed bandgap of the perovskite single crystals from 3.03 eV to 2.98 eV. In addition, the fabrication process of thin film single-crystalline solar cells at a µm scale is not yet completely optimized and has its own challenges, such as varying space between the two sandwiched substrates. This leads to a difference in thickness between various single crystals grown on a single substrate. Optimization could entail constant space between the substrates and increasing the amount of precursor between substrates to ensure larger crystals.[42] Furthermore, the thickness of as-grown single-crystalline thin films can be reduced by laser polishing as shown by Kedia et al.[43] This would result in thin single-crystalline layers of uniform thickness with a much smoother interface with the HTL. On the other hand, an increased volume of precursor solution with a lower concentration can help to avoid fast supersaturation and, hence, inhibit the multiple nucleation sites. In addition to that, careful post-treatments need to be defined that may help to improve the surface morphology of these single-crystalline thin films without detaching them from the substrates.

Finally, these devices, as a proof of concept, are further used as X-ray voltaic cells at different X-ray tube voltages. The performance of X-ray voltaic cells is governed by the maximum amount of energy deposited in the perovskite layer. Different factors influence the energy dosage of X-rays in the perovskite layer. The accelerating voltage of the incoming electrons in the X-ray tube and the thickness of the layers lying above the perovskite are very critical. If the accelerating voltage is too low, then most of the energy will be deposited into the front layers before the X-rays reach the perovskite layer. Similarly, if the accelerating voltage is too high, the X-rays will simply penetrate through the perovskite layer, and energy will be wasted. Keeping that in mind, in this work, the single-crystalline $MAPbCl_3$ devices have been exposed to X-rays from the Au contact side instead of from the glass side to avoid the energy deposition of X-rays in the thick glass substrate rather than in the perovskite layer.[20]

View Article Online
DOI: 10.1039/D5EL00087D

Since the energy of X-rays is significantly higher than the bandgap of the perovskites, $MAPbCl_3$, with its wide bandgap, can be used for X-ray voltaics. This results in the formation of hot carriers with high kinetic energy, which equilibrate themselves by dissipating the heat energy to the lattice instead of taking part in the power generation. Hence, I^- and Br^--based narrow bandgap perovskites are relatively less efficient for this purpose.[21] Here, $MAPbCl_3$ single-crystalline devices are measured as X-ray voltaic cells using a tungsten-based X-ray tube. Polycrystalline-$MAPbCl_3$ thin films cannot be employed for X-ray voltaics as their thickness is too low for X-rays to deposit any energy, resulting in no current signal. The X-ray beam is collimated using a 10 mm diameter aluminum slit and is directed on the X-ray voltaic cell. The complete schematic of the setup is shown in Figure 4a. An X-ray image of the X-ray voltaic cell is taken to make sure that the device lies within the focus of the X-ray beam, as shown in Figure 4b. The X-ray tube voltage is increased from 20 kV to 60 kV at a constant tube current of 1 mA to observe the influence of the tube voltage on the device performance. The corresponding power densities at each tube voltage (calculated via SpekPy[44] and counter checked by Monte Carlo Simulations[45]) range from 500 $\mu W cm^{-2}$ to 4900 $\mu W\ cm^{-2}$. Currently, our setup is restricted from going beyond 60 kV as it can cause adverse effects on the X-ray tube life.

View Article Online
DOI: 10.1039/D5EL00087D

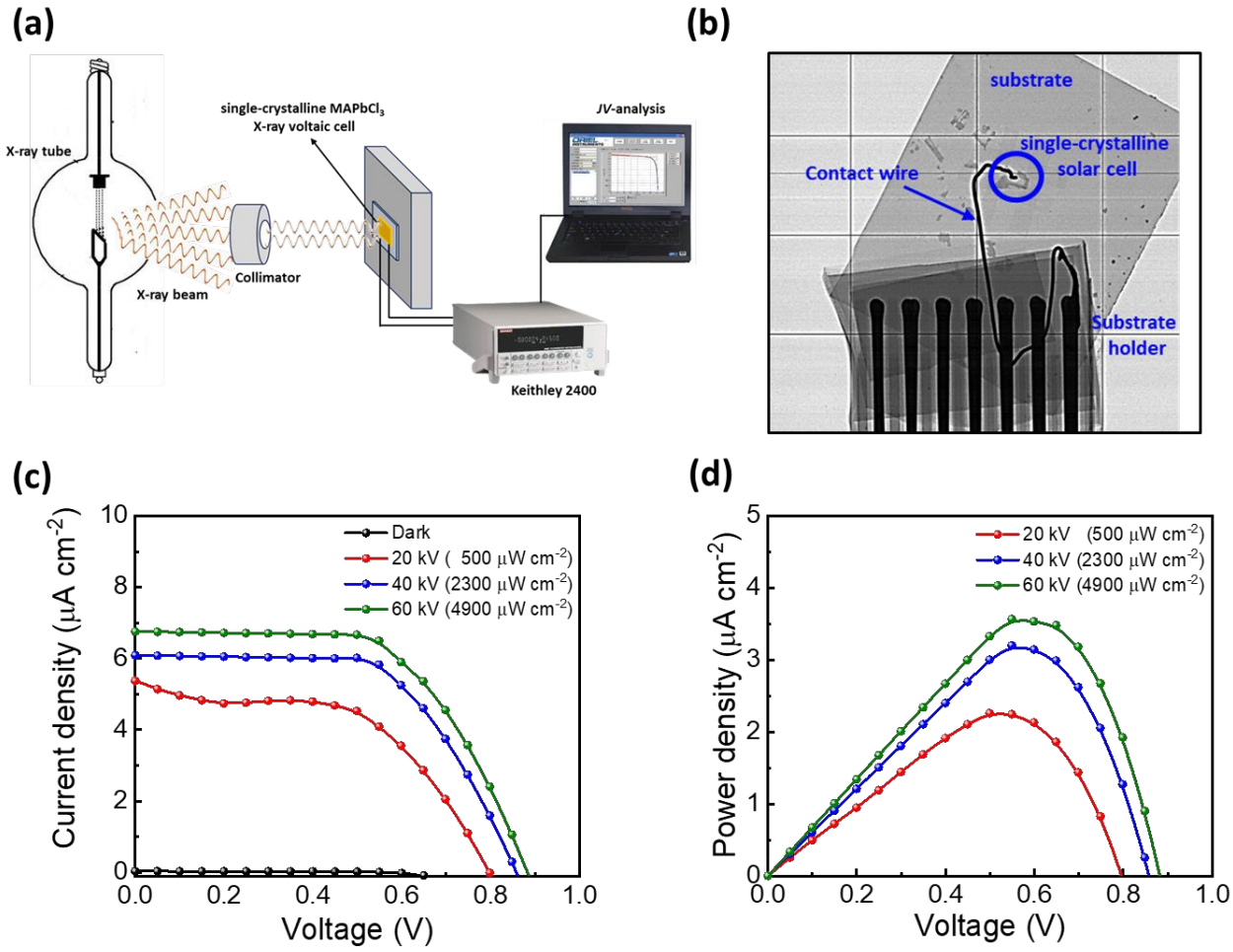

Figure 4 (a) Schematics of the X-ray voltaic setup consisting of a tungsten-based X-ray tube (b) X-ray image of a single-crystalline $MAPbCl_3$ solar cell on an ITO substrate contacted with a contact wire to measure *IV*-traces. (c) *JV*-curves of the champion single-crystalline $MAPbCl_3$ X-ray voltaic cells at different X-ray tube voltages corresponding to different illumination intensities (d) Output power curves of single-crystalline $MAPbCl_3$ X-ray voltaic cells at different X-ray tube voltages.

With increasing the tube voltage, the single-crystalline devices have shown improved X-ray voltaic parameters, as shown in Figure 4c: At a tube voltage of 20 kV equal to an input power density of 500 μW cm^{-2}, a J_{SC} of 5.40 μA cm^{-2}, along with a V_{OC} of 0.8 V, leading to an output power density of 2.26 μW cm^{-2}. For 40 kV (2300 μW cm^{-2}), J_{SC} and V_{OC} have increased to a value of 6.08 μA cm^{-2} and 0.86 V, respectively, with a power conversion of 3.2 μW cm^{-2}. The highest V_{OC} of 0.89 V with a J_{SC} of 6.73 μA cm^{-2} is obtained at a tube voltage of 60 kV (4900 μW cm^{-2}) with an output power density of 3.57 μW cm^{-2}. The output power curves corresponding to different X-ray input powers have been shown in Figure 4d. To the best of our knowledge, this is the highest output

View Article Online
DOI: 10.1039/D5EL00087D

power achieved by perovskite X-ray voltaic cells. Previously, Moazzezi et al. have reported an output power of 0.33 μW cm^{-2} for single-crystalline $MAPbI_3$-based X-ray voltaic cells.[22] In a similar approach, an output power of ~ 0.14 μW has been reported for AlGaInP based X-ray voltaics.[46] Our findings further strengthen that wide bandgap perovskites exhibit significantly superior performance compared to narrow bandgap ones, when exposed to radiant sources like X-rays.[21] This is contrary to their trend under one sun condition, where photovoltaic power conversion decreases with the increase in bandgap. This efficient harvesting of radiant energy shows the potential of $MAPbCl_3$ to power low-power devices such as micro-electro-mechanical systems (MEMS) during space missions. These self-powered X-ray voltaic devices also eliminate the need for a battery to power the devices.[46]

Moreover, compared to $MAPbI_3$ and $MAPbBr_3$, $MAPbCl_3$ exhibits superior intrinsic stability due to its more negative enthalpy of formation,[47,48] stronger Pb–Cl bonds that inhibit defect formation and degradation,[49,50] and enhanced resistance to moisture.[51] These characteristics make it particularly well-suited for the environments and applications discussed above. At the same time, there is still significant scope for improving the device's performance under X-ray irradiation. For example, the thickness of perovskite, ETL, HTL, and metallic thin films could be further optimized such that the maximum energy deposition occurs in the absorber layer. Moreover, standardized measurement conditions for X-ray voltaics are also very crucial for enhancing their performance.

Conclusion

In conclusion, we demonstrate the potential of $MAPbCl_3$ perovskite in the form of single-crystalline thin films for both photo and X-ray voltaics. Our results show that, compared to polycrystalline thin films, high-quality single-crystalline $MAPbCl_3$ thin films can be crystallized out without any annealing or passive step. These single-crystalline thin films result in a V_{OC} of 1.64 V and a PCE of 1.1%. At the same time, currently, the increased thickness of single-crystalline thin films results in enhanced non-radiative recombination processes affecting the overall diffusion of the charge carriers, leading to a relatively lower V_{OC}. As a proof of concept, these single-crystalline $MAPbCl_3$ thin films are further employed as X-ray voltaic cells. At a tube voltage of 60 kV, this leads to a V_{OC} of 0.89 V and a remarkable output power of 3.57 μW cm^{-2}, highlighting the potential of the widest bandgap perovskites for novel use cases beyond solar applications. For

View Article Online
DOI: 10.1039/D5EL00087D

277 example, $MAPbCl_3$-based X-ray voltaic cells could be utilized to harvest energy from nuclear
278 waste.

279

View Article Online
DOI: 10.1039/D5EL00087D

Acknowledgements

M.S., W.Z., and M.M.B. thank the Helmholtz Young Investigator Group FRONTRUNNER. M. S. acknowledges funding by ProperPhotoMile. Project ProperPhotoMile is supported under the umbrella of SOLAR-ERA.NET Cofund 2 by the Spanish Ministry of Science and Education and the AEI under the project PCI2020-112185 and CDTI project number IDI-20210171; the Federal Ministry for Economic Affairs and Energy on the basis of a decision by the German Bundestag project numbers FKZ 03EE1070B and FKZ 03EE1070A and the Israel Ministry of Energy with project number 220-11-031. SOLAR-ERA.NET is supported by the European Commission within the EU Framework Programme for Research and Innovation HORIZON 2020 (Cofund ERA-NET Action, No. 786483), funded by the European Union. The views and opinions expressed are, however, those of the author(s) only and do not necessarily reflect those of the European Union or the European Research Council Executive Agency (ERCEA). Neither the European Union nor the granting authority can be held responsible for them. M.S. acknowledges funding from the European Research Council under the Horizon Europe program (LOCAL-HEAT, grant agreement no. 101041809). M. S. thanks the German Research Foundation (DFG) for funding (SPP2196, 431314977/GRK 2642). M. S. acknowledges funding from the German Bundesministerium für Bildung and Forschung (BMBF), project "NETPEC" (01LS2103E). M.I.S. thanks the Natural Sciences and Engineering Research Council of Canada (ALLRP 566552 - 21), the Canadian Foundation for Innovation (40326), and the B.C. Knowledge Development Fund (806169) for their support in operations and infrastructure. Y.H. acknowledges Japan Society for the Promotion of Science (JSPS) Overseas Research Fellow, acknowledges the financial support from JSPS.

Conflicts of interest

There are no conflicts to declare.

References

(1) Kojima, A.; Teshima, K.; Shirai, Y.; Miyasaka, T. Organometal Halide Perovskites as Visible-Light Sensitizers for Photovoltaic Cells. J. Am. Chem. Soc. 2009, 131 (17), 6050–6051. https://doi.org/10.1021/ja809598r.

(2) Saliba, M.; Matsui, T.; Seo, J.-Y.; Domanski, K.; Correa-Baena, J.-P.; Khaja Nazeeruddin, M.; M. Zakeeruddin, S.; Tress, W.; Abate, A.; Hagfeldt, A.; Grätzel, M. Cesium-Containing Triple

View Article Online
DOI: 10.1039/D5EL00087D

Cation Perovskite Solar Cells: Improved Stability, Reproducibility and High Efficiency. Energy & Environmental Science 2016, 9 (6), 1989–1997. https://doi.org/10.1039/C5EE03874J.

(3) Rong, Y.; Hu, Y.; Mei, A.; Tan, H.; Saidaminov, M. I.; Seok, S. I.; McGehee, M. D.; Sargent, E. H.; Han, H. Challenges for Commercializing Perovskite Solar Cells. Science 2018, 361 (6408), eaat8235. https://doi.org/10.1126/science.aat8235.

(4) Park, S. M.; Wei, M.; Xu, J.; Atapattu, H. R.; Eickemeyer, F. T.; Darabi, K.; Grater, L.; Yang, Y.; Liu, C.; Teale, S.; Chen, B.; Chen, H.; Wang, T.; Zeng, L.; Maxwell, A.; Wang, Z.; Rao, K. R.; Cai, Z.; Zakeeruddin, S. M.; Pham, J. T.; Risko, C. M.; Amassian, A.; Kanatzidis, M. G.; Graham, K. R.; Grätzel, M.; Sargent, E. H. Engineering Ligand Reactivity Enables High-Temperature Operation of Stable Perovskite Solar Cells. Science 2023, 381 (6654), 209–215. https://doi.org/10.1126/science.adi4107.

(5) Marinova, N.; Valero, S.; Delgado, J. L. Organic and Perovskite Solar Cells: Working Principles, Materials and Interfaces. Journal of Colloid and Interface Science 2017, 488, 373–389. https://doi.org/10.1016/j.jcis.2016.11.021.

(6) Daboczi, M.; Hamilton, I.; Xu, S.; Luke, J.; Limbu, S.; Lee, J.; McLachlan, M. A.; Lee, K.; Durrant, J. R.; Baikie, I. D.; Kim, J.-S. Origin of Open-Circuit Voltage Losses in Perovskite Solar Cells Investigated by Surface Photovoltage Measurement. ACS Appl. Mater. Interfaces 2019, 11 (50), 46808–46817. https://doi.org/10.1021/acsami.9b16394.

(7) Tress, W. Perovskite Solar Cells on the Way to Their Radiative Efficiency Limit – Insights Into a Success Story of High Open-Circuit Voltage and Low Recombination. Advanced Energy Materials 2017, 7 (14), 1602358. https://doi.org/10.1002/aenm.201602358.

(8) Zia, W.; Malekshahi Byranvand, M.; Rudolph, T.; Rai, M.; Kot, M.; Das, C.; Kedia, M.; Zohdi, M.; Zuo, W.; Yeddu, V.; Saidaminov, M. I.; Flege, J. I.; Kirchartz, T.; Saliba, M. MAPbCl3 Light Absorber for Highest Voltage Perovskite Solar Cells. ACS Energy Lett. 2024, 9 (3), 1017–1024. https://doi.org/10.1021/acsenergylett.3c02777.

(9) Liu, D.; Yang, C.; Lunt, R. R. Halide Perovskites for Selective Ultraviolet-Harvesting Transparent Photovoltaics. Joule 2018, 2 (9), 1827–1837. https://doi.org/10.1016/j.joule.2018.06.004.

(10) Chen, Z.; Li, C.; Zhumekenov, A. A.; Zheng, X.; Yang, C.; Yang, H.; He, Y.; Turedi, B.; Mohammed, O. F.; Shen, L.; Bakr, O. M. Solution-Processed Visible-Blind Ultraviolet Photodetectors with Nanosecond Response Time and High Detectivity. Advanced Optical Materials 2019, 7 (19), 1900506. https://doi.org/10.1002/adom.201900506.

(11) Hsu, H.-P.; Li, L.-C.; Shellaiah, M.; Sun, K. W. Structural, Photophysical, and Electronic Properties of CH3NH3PbCl3 Single Crystals. Sci Rep 2019, 9 (1), 13311. https://doi.org/10.1038/s41598-019-49926-z.

(12) Y. Alsalloum, A.; Turedi, B.; Almasabi, K.; Zheng, X.; Naphade, R.; D. Stranks, S.; F. Mohammed, O.; M. Bakr, O. 22.8%-Efficient Single-Crystal Mixed-Cation Inverted Perovskite

View Article Online
DOI: 10.1039/D5EL00087D

Solar Cells with a near-Optimal Bandgap. Energy & Environmental Science 2021, 14 (4), 2263–2268. https://doi.org/10.1039/D0EE03839C.

(13) Peng, W.; Wang, L.; Murali, B.; Ho, K.-T.; Bera, A.; Cho, N.; Kang, C.-F.; Burlakov, V. M.; Pan, J.; Sinatra, L.; Ma, C.; Xu, W.; Shi, D.; Alarousu, E.; Goriely, A.; He, J.-H.; Mohammed, O. F.; Wu, T.; Bakr, O. M. Solution-Grown Monocrystalline Hybrid Perovskite Films for Hole-Transporter-Free Solar Cells. Advanced Materials 2016, 28 (17), 3383–3390. https://doi.org/10.1002/adma.201506292.

(14) Rao, H.-S.; Chen, B.-X.; Wang, X.-D.; Kuang, D.-B.; Su, C.-Y. A Micron-Scale Laminar MAPbBr 3 Single Crystal for an Efficient and Stable Perovskite Solar Cell. Chemical Communications 2017, 53 (37), 5163–5166. https://doi.org/10.1039/C7CC02447A.

(15) Moazzezi, P.; Yeddu, V.; Cheong, I. T.; Kokaba, M. R.; Dayneko, S.; Ahmed, Y.; Saidaminov, M. I. Discovery of Perovskite Cosolvency and Undoped FAPbI3 Single-Crystal Solar Cells Fabricated in Ambient Air. J. Am. Chem. Soc. 2025, 147 (12), 10203–10211. https://doi.org/10.1021/jacs.4c15716.

(16) Chen, Z.; Turedi, B.; Alsalloum, A. Y.; Yang, C.; Zheng, X.; Gereige, I.; AlSaggaf, A.; Mohammed, O. F.; Bakr, O. M. Single-Crystal MAPbI3 Perovskite Solar Cells Exceeding 21% Power Conversion Efficiency. ACS Energy Lett. 2019, 4 (6), 1258–1259. https://doi.org/10.1021/acsenergylett.9b00847.

(17) Alsalloum, A. Y.; Turedi, B.; Zheng, X.; Mitra, S.; Zhumekenov, A. A.; Lee, K. J.; Maity, P.; Gereige, I.; AlSaggaf, A.; Roqan, I. S.; Mohammed, O. F.; Bakr, O. M. Low-Temperature Crystallization Enables 21.9% Efficient Single-Crystal MAPbI3 Inverted Perovskite Solar Cells. ACS Energy Lett. 2020, 5 (2), 657–662. https://doi.org/10.1021/acsenergylett.9b02787.

(18) Sakhatskyi, K.; Turedi, B.; Matt, G. J.; Wu, E.; Sakhatska, A.; Bartosh, V.; Lintangpradipto, M. N.; Naphade, R.; Shorubalko, I.; Mohammed, O. F.; Yakunin, S.; Bakr, O. M.; Kovalenko, M. V. Stable Perovskite Single-Crystal X-Ray Imaging Detectors with Single-Photon Sensitivity. Nat. Photon. 2023, 17 (6), 510–517. https://doi.org/10.1038/s41566-023-01207-y.

(19) He, Y.; Liu, Z.; McCall, K. M.; Lin, W.; Chung, D. Y.; Wessels, B. W.; Kanatzidis, M. G. Perovskite CsPbBr3 Single Crystal Detector for Alpha-Particle Spectroscopy. Nuclear Instruments and Methods in Physics Research Section A: Accelerators, Spectrometers, Detectors and Associated Equipment 2019, 922, 217–221. https://doi.org/10.1016/j.nima.2019.01.008.

(20) Song, Z.; Zhao, C.; Liao, F.; Zhao, Y. Perovskite-Betavoltaic Cells: A Novel Application of Organic–Inorganic Hybrid Halide Perovskites. ACS Appl. Mater. Interfaces 2019, 11 (36), 32969–32977. https://doi.org/10.1021/acsami.9b09952.

(21) Li, G.; Zhao, C.; Liu, Y.; Ren, J.; Zhang, Z.; Di, H.; Jiang, W.; Mei, J.; Zhao, Y. High-Performance Perovskite Betavoltaics Employing High-Crystallinity MAPbBr3 Films. ACS Omega 2021, 6 (30), 20015–20025. https://doi.org/10.1021/acsomega.1c03053.

View Article Online
DOI: 10.1039/D5EL00087D

(22) Moazzezi, P.; Yeddu, V.; Dayneko, S.; Haruta, Y.; Kokaba, M. R.; Richtsmeier, D.; Ahmed, Y.; Amaro, A.; Bazalova-Carter, M.; Navarrete-López, A. M.; Saidaminov, M. I. Kinetics of Space-Confined Inverse Temperature Crystallization: Gradients Enlarge Thin Perovskite Single Crystals. ACS Materials Lett. 2024, 6 (8), 3557–3563. https://doi.org/10.1021/acsmaterialslett.4c00740.

(23) Cheng, X.; Yang, S.; Cao, B.; Tao, X.; Chen, Z. Single Crystal Perovskite Solar Cells: Development and Perspectives. Advanced Functional Materials 2020, 30 (4), 1905021. https://doi.org/10.1002/adfm.201905021.

(24) Ghasemi, M.; Yuan, S.; Fan, J.; Jia, B.; Wen, X. Challenges in the Development of Metal-Halide Perovskite Single Crystal Solar Cells. Journal of Materials Chemistry A 2023, 11 (8), 3822–3848. https://doi.org/10.1039/D2TA08827D.

(25) Siekmann, J.; Ravishankar, S.; Kirchartz, T. Apparent Defect Densities in Halide Perovskite Thin Films and Single Crystals. ACS Energy Lett. 2021, 6 (9), 3244–3251. https://doi.org/10.1021/acsenergylett.1c01449.

(26) Ravishankar, S.; Unold, T.; Kirchartz, T. Comment on "Resolving Spatial and Energetic Distributions of Trap States in Metal Halide Perovskite Solar Cells." Science 2021, 371 (6532), eabd8014. https://doi.org/10.1126/science.abd8014.

(27) Wu, Y.; Feng, J.; Yang, Z.; Liu, Y.; Liu, S. (Frank). Halide Perovskite: A Promising Candidate for Next-Generation X-Ray Detectors. Advanced Science 2023, 10 (1), 2205536. https://doi.org/10.1002/advs.202205536.

(28) Buin, A.; Comin, R.; Xu, J.; Ip, A. H.; Sargent, E. H. Halide-Dependent Electronic Structure of Organolead Perovskite Materials. Chem. Mater. 2015, 27 (12), 4405–4412. https://doi.org/10.1021/acs.chemmater.5b01909.

(29) Maculan, G.; Sheikh, A. D.; Abdelhady, A. L.; Saidaminov, M. I.; Haque, M. A.; Murali, B.; Alarousu, E.; Mohammed, O. F.; Wu, T.; Bakr, O. M. CH3NH3PbCl3 Single Crystals: Inverse Temperature Crystallization and Visible-Blind UV-Photodetector. J. Phys. Chem. Lett. 2015, 6 (19), 3781–3786. https://doi.org/10.1021/acs.jpclett.5b01666.

(30) Zheng, E.; Yuh, B.; Tosado, G. A.; Yu, Q. Solution-Processed Visible-Blind UV-A Photodetectors Based on $CH_3NH_3PbCl_3$ Perovskite Thin Films. J. Mater. Chem. C 2017, 5 (15), 3796–3806. https://doi.org/10.1039/C7TC00639J.

(31) Chen, Z.; Dong, Q.; Liu, Y.; Bao, C.; Fang, Y.; Lin, Y.; Tang, S.; Wang, Q.; Xiao, X.; Bai, Y.; Deng, Y.; Huang, J. Thin Single Crystal Perovskite Solar Cells to Harvest Below-Bandgap Light Absorption. Nat Commun 2017, 8 (1), 1890. https://doi.org/10.1038/s41467-017-02039-5.

(32) Hutter, E. M.; Gélvez-Rueda, M. C.; Osherov, A.; Bulović, V.; Grozema, F. C.; Stranks, S. D.; Savenije, T. J. Direct–Indirect Character of the Bandgap in Methylammonium Lead Iodide Perovskite. Nature Mater 2017, 16 (1), 115–120. https://doi.org/10.1038/nmat4765.

View Article Online
DOI: 10.1039/D5EL00087D

(33) Motta, C.; El-Mellouhi, F.; Kais, S.; Tabet, N.; Alharbi, F.; Sanvito, S. Revealing the Role of Organic Cations in Hybrid Halide Perovskite CH3NH3PbI3. Nat Commun 2015, 6 (1), 7026. https://doi.org/10.1038/ncomms8026.

(34) Wang, T.; Daiber, B.; M. Frost, J.; A. Mann, S.; C. Garnett, E.; Walsh, A.; Ehrler, B. Indirect to Direct Bandgap Transition in Methylammonium Lead Halide Perovskite. Energy & Environmental Science 2017, 10 (2), 509–515. https://doi.org/10.1039/C6EE03474H.

(35) Chen, G.; Liu, X.; An, J.; Wang, S.; Zhao, X.; Gu, Z.; Yuan, C.; Xu, X.; Bao, J.; Hu, H.-S.; Li, J.; Wang, X. Nucleation-Mediated Growth of Chiral 3D Organic–Inorganic Perovskite Single Crystals. Nat. Chem. 2023, 15 (11), 1581–1590. https://doi.org/10.1038/s41557-023-01290-2.

(36) Sproul, A. B. Dimensionless Solution of the Equation Describing the Effect of Surface Recombination on Carrier Decay in Semiconductors. Journal of Applied Physics 1994, 76 (5), 2851–2854. https://doi.org/10.1063/1.357521.

(37) Singh, P.; Ravindra, N. M. Temperature Dependence of Solar Cell Performance—an Analysis. Solar Energy Materials and Solar Cells 2012, 101, 36–45. https://doi.org/10.1016/j.solmat.2012.02.019.

(38) Marti, A.; Balenzategui, J. L.; Reyna, R. F. Photon Recycling and Shockley's Diode Equation. Journal of Applied Physics 1997, 82 (8), 4067. https://doi.org/10.1063/1.365717.

(39) Zonno, I.; Krogmeier, B.; Katte, V.; Lübke, D.; Martinez-Otero, A.; Kirchartz, T. Discriminating between Surface and Bulk Recombination in Organic Solar Cells by Studying the Thickness Dependence of the Open-Circuit Voltage. Applied Physics Letters 2016, 109 (18), 183301. https://doi.org/10.1063/1.4966613.

(40) Lübke, D.; Hartnagel, P.; Hülsbeck, M.; Kirchartz, T. Understanding the Thickness and Light-Intensity Dependent Performance of Green-Solvent Processed Organic Solar Cells. ACS Mater. Au 2023, 3 (3), 215–230. https://doi.org/10.1021/acsmaterialsau.2c00070.

(41) Single-Crystal Perovskite Solar Cells Exhibit Close to Half A Millimeter Electron-Diffusion Length - Turedi - 2022 - Advanced Materials - Wiley Online Library. https://onlinelibrary.wiley.com/doi/abs/10.1002/adma.202202390 (accessed 2023-11-09).

(42) De Marco, L.; Nasti, G.; Abate, A.; Rizzo, A. Perovskite Single-Crystal Solar Cells: Advances and Challenges. Solar RRL 2022, 6 (7), 2101085. https://doi.org/10.1002/solr.202101085.

(43) Kedia, M.; Rai, M.; Phirke, H.; Aranda, C. A.; Das, C.; Chirvony, V.; Boehringer, S.; Kot, M.; Byranvand, M. M.; Flege, J. I.; Redinger, A.; Saliba, M. Light Makes Right: Laser Polishing for Surface Modification of Perovskite Solar Cells. ACS Energy Lett. 2023, 8 (6), 2603–2610. https://doi.org/10.1021/acsenergylett.3c00469.

View Article Online
DOI: 10.1039/D5EL00087D

(44) Poludniowski, G.; Omar, A.; Bujila, R.; Andreo, P. Technical Note: SpekPy v2.0—a Software Toolkit for Modeling x-Ray Tube Spectra. Medical Physics 2021, 48 (7), 3630–3637. https://doi.org/10.1002/mp.14945.

(45) Bazalova-Carter, M.; Esplen, N. On the Capabilities of Conventional X-Ray Tubes to Deliver Ultra-High (FLASH) Dose Rates. Medical Physics 2019, 46 (12), 5690–5695. https://doi.org/10.1002/mp.13858.

(46) Wu, Y.; Xu, Z.; Liu, Y.; Jiang, T.; San, H.; Tang, X. Research on X-Ray-Based Energy Conversion Technology and Assessment of Application Prospect. Sustainable Energy Technologies and Assessments 2023, 60, 103552. https://doi.org/10.1016/j.seta.2023.103552.

(47) Senocrate, A.; Kim, G. Y.; Grätzel, M.; Maier, J. Thermochemical Stability of Hybrid Halide Perovskites. ACS Energy Lett. 2019, 4 (12), 2859–2870. https://doi.org/10.1021/acsenergylett.9b01605.

(48) Brunetti, B.; Cavallo, C.; Ciccioli, A.; Gigli, G.; Latini, A. On the Thermal and Thermodynamic (In)Stability of Methylammonium Lead Halide Perovskites. Sci Rep 2016, 6 (1), 31896. https://doi.org/10.1038/srep31896.

(49) Caputo, M.; Cefarin, N.; Radivo, A.; Demitri, N.; Gigli, L.; Plaisier, J. R.; Panighel, M.; Di Santo, G.; Moretti, S.; Giglia, A.; Polentarutti, M.; De Angelis, F.; Mosconi, E.; Umari, P.; Tormen, M.; Goldoni, A. Electronic Structure of MAPbI3 and MAPbCl3: Importance of Band Alignment. Sci Rep 2019, 9, 15159. https://doi.org/10.1038/s41598-019-50108-0.

(50) McGovern, L.; Futscher, M. H.; Muscarella, L. A.; Ehrler, B. Understanding the Stability of MAPbBr3 versus MAPbI3: Suppression of Methylammonium Migration and Reduction of Halide Migration. J Phys Chem Lett 2020, 11 (17), 7127–7132. https://doi.org/10.1021/acs.jpclett.0c01822.

(51) Jong, U.-G.; Yu, C.-J.; Ri, G.-C.; McMahon, A. P.; Harrison, N. M.; Barnes, P. R. F.; Walsh, A. Influence of Water Intercalation and Hydration on Chemical Decomposition and Ion Transport in Methylammonium Lead Halide Perovskites. arXiv October 14, 2017. https://doi.org/10.48550/arXiv.1708.07608.

View Article Online
DOI: 10.1039/D5EL00087D

Data availability

The data will be available upon reasonable request.